



Dynamics and heat transfer in a quasi-two-dimensional MHD flow past a circular cylinder in a duct at high Hartmann number

Wisam K. Hussam, Mark C. Thompson, Gregory J. Sheard*

Department of Mechanical and Aerospace Engineering, Monash University, VIC 3800, Australia

ARTICLE INFO

Article history:

Received 12 August 2010

Received in revised form 8 November 2010

Keywords:

Magnetohydrodynamics

Quasi two-dimensional model

Channel flow

Circular cylinder

Blockage ratio

ABSTRACT

The fluid flow and heat transfer of a liquid metal past a circular cylinder in a rectangular duct (width-to-height aspect ratio of 2) under a strong transverse magnetic field is studied numerically using a quasi-two-dimensional model. Transition from steady to unsteady flow regimes is determined as a function of Hartmann number and blockage ratio, as are Strouhal number, and the heat transfer from the heated wall to the fluid. Downstream cross-stream mixing induced by the cylinder wake was found to increase heat transfer by more than a factor of two in some cases.

© 2010 Elsevier Ltd. All rights reserved.

1. Introduction

The study of liquid metal flow in ducts in the presence of a transverse magnetic field has received attention because of its application to important technologies such as metallurgical processing, hydrodynamic generators, pumps, and blood flow meters. The primary application motivating this study is magnetic confinement fusion reactors, where liquid metal is used as a coolant and as a breeder material [1]. In most fusion reactor blankets the liquid metal circulates in an electrically insulated duct perpendicular to the applied magnetic field. The motion of liquid metal in a strong magnetic field induces electric currents, which in turn interact with the magnetic field resulting in a Lorentz force. This has a significant effect on the velocity distribution and the turbulence characteristics, and exerts a retarding force on the flow.

Under a strong magnetic field the flow is characterized by a laminar flow structure as velocity fluctuations in the direction of the magnetic field are strongly damped. Therefore, the heat transfer in the ducts of the first wall where large amount of heating power must be removed is dramatically decreased [2]. However, the two-dimensional turbulence that consists of vortices with axes parallel to the magnetic field are not significantly damped [3]. This turbulence could be used to enhance the heat transfer by using turbulence promoters such as a circular cylinder placed inside the duct of a blanket.

In the absence of a magnetic field, the flow past a circular cylinder depends on the Reynolds number and whether the flow is con-

fined or unconfined. In an unconfined domain, the flow depends on Reynolds number as the sole control parameter. As Reynolds number increases, the flow becomes unstable first to two-dimensional disturbances, then three-dimensional instability modes [4]. At Reynolds numbers $Re \lesssim 46$, the flow is steady, and the wake comprises a counter-rotating pair of vortices attached to the rear of the cylinder. Beyond $Re \approx 46$, this flow becomes temporally unstable, with vortices shed periodically from alternating sides of the cylinder—the classical Kármán vortex street. This regime continues up to $Re \approx 180$, beyond which the flow becomes three-dimensional (for details see Williamson [4], Zdravkovich [5]).

In contrast, when the circular cylinder is confined in a plane channel, the nature and stability of the resulting flow changes significantly. The effect of wall confinement on the stability of the flow and flow parameters such as drag and lift coefficients, Strouhal number, and Nusselt number have been investigated by Coutanceau and Bouard [6], Chen et al. [7], Behr et al. [8], Anagnosopoulos et al. [9], Zovatto and Pedrizzetti [10], Khan et al. [11], Chakraborty et al. [12], Sahin and Owens [13], Cliffe and Tavener [14], Mettu et al. [15]. In this configuration, the blockage ratio (cylinder diameter to channel width) is an additional control parameter. Due to the additional dissipation at the confining walls, the transition from steady to unsteady flow is delayed and occurs at Reynolds numbers higher than that in unconfined flow.

For the liquid metals used in the fusion blanket, the Hartmann number (Ha , the ratio between electromagnetic and viscous forces) and the interaction parameter ($N = Ha^2/Re$, the ratio of electromagnetic to inertial forces) are very high (i.e. $Ha \gg 1, N \gg 1$). This implies that the electromagnetic forces outweigh the viscous forces, and the flow in a rectangular duct can be split into one or

* Corresponding author.

E-mail address: Greg.Sheard@monash.edu (G.J. Sheard).

Nomenclature

a	channel half-height	St_c	Strouhal number at Re_c
A	instability mode amplitude	ΔT	temperature difference between channel side walls
B	magnetic field	t	time
C_d	cylinder drag coefficient	T	temperature field
C_l	cylinder lift coefficient	T_f	bulk fluid temperature
d	cylinder diameter	T_o	temperature of fluid entering channel
f	wake oscillation frequency	T_w	temperature of hot channel side-wall
F'_d	drag force per unit span	u	streamwise component of velocity
h	channel width	\mathbf{u}	velocity vector field
Ha	Hartmann number	U_o	peak inlet velocity
HI	percentage heat transfer increment	x	Cartesian coordinate in flow direction
L	length along heated bottom wall	x_u	length to upstream boundary
N	interaction parameter	x_d	length to downstream boundary
N_{el}	number of spectral elements in mesh	y	Cartesian coordinate across channel
Nu	time-averaged Nusselt number		
Nu_0	time-averaged Nusselt number in empty channel		
Nu_w	local Nusselt number		
$\bar{N}u_w$	time-average of local Nusselt number		
ΔP	pressure drop across channel		
p	pressure		
Pe	Peclet number		
Re	Reynolds number		
Re_c	critical Reynolds number for onset of vortex shedding		
St	Strouhal number		

			Greek symbol
			β blockage ratio
			δ_H Hartmann boundary layer thickness
			δ_S Shercliff boundary layer thickness
			ν kinematic viscosity
			ρ fluid density
			σ magnetic permeability
			ω vorticity in $x-y$ plane

more quasi-inviscid core flows, separated by thin boundary or shear layers of two types. The core occupies almost the whole duct cross section. In this region there is a balance between the pressure and the Lorentz force. In the boundary layer region, viscous forces are balanced by Lorentz forces. The boundary layer adjacent to the wall perpendicular to the magnetic field is known as the Hartmann layer, and is characterized by an exponential decay of the velocity towards the wall. Its thickness scales as $\delta_H \sim O(Ha^{-1})$ [16]. The boundary layer adjacent to the wall parallel to the magnetic field is known as a Shercliff layer (or side layer), with a thickness that scales with $\delta_S \sim Ha^{-1/2}$ [16].

The magnetic field may intensify vortices parallel to the magnetic field. The effect of the magnetic field on the evolution of the vortices has been investigated theoretically by Davidson [17], Pothierat et al. [18], Sommeria and Moreau [19] and experimentally by Alboussiere et al. [20], Andreev and Kolesnikov [21], Burr et al. [22], Klein et al. [23], Buhler [24]. The properties of such flows was first studied by Kolesnikov and Tsinober [25] in decaying grid turbulence, and later by Moreau and Sommeria [26] in the electromagnetically forced regimes. The mechanisms are explained by Sommeria and Moreau [19], who showed that the velocity components perpendicular to the magnetic field are dissipated by strong joule heating dissipation, except in the Hartmann layer where the turbulent fluctuations are weakly damped in that direction.

In order to initiate turbulence, Buhler [24] numerically investigated the transition between stationary flow and quasi two-dimensional vortex structures for the shear flow profile which is generated by the insertion two thin strips of different conductivity in the transverse and streamwise directions. The resulting flow profile was similar to the Kármán vortex street behind a circular cylinder without a magnetic field. However, another mechanism for producing vortices in an insulated channel is by using turbulence promoters such as cylindrical or rectangular obstacles placed parallel to the direction of the applied magnetic field. This approach has been investigated experimentally by Kit et al. [27] and Kolesnikov and Tsinober [28]. The shape of vortex street in an open channel with only one Hartmann wall under a strong mag-

netic field has been investigated experimentally by Papailiou [29]. He observed that under the effect of a magnetic field, the wake becomes narrower than that without a magnetic field. In addition, it has been shown that the distance between the vortices in the main stream direction was reduced and a row of vortices were organized downstream. However, the effect of the magnetic field aligned with the cylinder axis on Strouhal number was weak.

More recently, Frank et al. [30] investigated experimentally the wake behind a circular cylinder of quasi two-dimensional liquid metal flow in a rectangular duct for the condition of high Reynolds and Hartmann number. The value of Reynolds number was within the range $100 \leq Re \leq 10,000$, and for the Hartmann number $500 \leq Ha \leq 1200$, which gave values of interaction parameter N between 10 and 576. The blockage ratio was set to $\beta = 0.1$. The experimental results revealed that there is a linear dependence of the critical Reynolds number on Hartmann number for the onset of time-dependent vortex shedding. They conclude that the dissipation of vortical energy is achieved by the quasi two-dimensional linear damping term, which leads to a continuous decrease in vortex intensity with downstream distance.

For the same configuration Muck et al. [31] have performed three-dimensional numerical simulations for liquid metal flows around a square cylinder in a rectangular duct. The interaction parameter was varied in the range $0 \leq N \leq 36$ and the Hartmann number in the range $0 \leq Ha \leq 85$. The numerical simulation was carried out for two fixed values of Reynolds number, 200 and 250. The numerical results were in a good agreement with the experimental obtained by Frank et al. [30].

Dousset and Pothierat [32] studied numerically the wake behind a circular cylinder for a quasi two-dimensional liquid metal flow placed in a square duct under a strong magnetic field parallel to the cylinder axis. Their simulations were carried out for Reynolds numbers $Re \leq 6000$, Hartmann numbers $0 \leq Ha \leq 2160$, and blockage ratio $\beta = 0.25$. The results revealed that the transition between the flow regimes were controlled by the linear friction term proportional to Re/Ha . Also, it has been found that the break up of the two-dimensional vortex street occurs at $Re = 5000$.

The aim of the present work is to study the dynamics and heat transfer characteristics of a quasi-two-dimensional magnetohydrodynamic flow past a confined circular cylinder with a strong magnetic field for $50 \leq Re \leq 3000$, $0 \leq Ha \leq 1200$, and $0.1 \leq \beta \leq 0.4$. In particular, the effect of Hartmann number and blockage ratio on the structure of the flow and heat transfer will be investigated.

2. Mathematical formulation

The system of interest is a rectangular duct confining a circular cylinder placed at the centre of the duct parallel to the transverse direction and perpendicular to the flow direction. The duct walls and the cylinder are assumed to be electrically insulated. A homogeneous vertical magnetic field with a strength B is imposed along the cylinder axis. One of the walls oriented parallel to the magnetic field is heated to a constant wall temperature T_w whereas the other surfaces are thermally insulated. For a high Hartmann number, the magnetic Reynolds number Re_m , which represents the ratio between the induced and the applied magnetic field is very small. Thus, the induced magnetic field is negligible and the resulting magnetic field is imposed in the z -direction only. Under these conditions the flow is quasi two-dimensional and consists of a core region, where the velocity is invariant along the direction of the magnetic field, and a thin Hartmann layer at the wall perpendicular to the magnetic field. The quasi two-dimensional model has been derived by Sommeria and Moreau [19] and Sheard et al. [33], by averaging the flow quantities along the magnetic field direction, as shown in Fig. 1.

In this case the non-dimensional magnetohydrodynamic equations of continuity, momentum, and energy reduce to

$$\nabla \cdot \mathbf{u} = 0, \quad (1)$$

$$\frac{\partial \mathbf{u}}{\partial t} + (\mathbf{u} \cdot \nabla) \mathbf{u} + \nabla p = \frac{1}{Re} \nabla^2 \mathbf{u} - \frac{d}{a} \frac{Ha}{Re} \mathbf{u}, \quad (2)$$

$$\frac{\partial T}{\partial t} + (\mathbf{u} \cdot \nabla) T = \frac{1}{Pe} \nabla^2 T, \quad (3)$$

where \mathbf{u} , p and T are the velocity, pressure, and temperature fields, respectively, projected onto the x - y plane. Lengths are scaled by the cylinder diameter d , pressure by ρU_0^2 , where ρ is the density and U_0 is the peak inlet velocity, time by d/U_0 , and temperature by the imposed temperature difference between the bottom and top walls, ΔT [22,34]. It is noted that the energy equation is sometimes written to include terms describing the effects of viscous dissipation and Joule heating (e.g., see [35]). However, here these terms are omitted (following [22,36] and others), after an order of magnitude

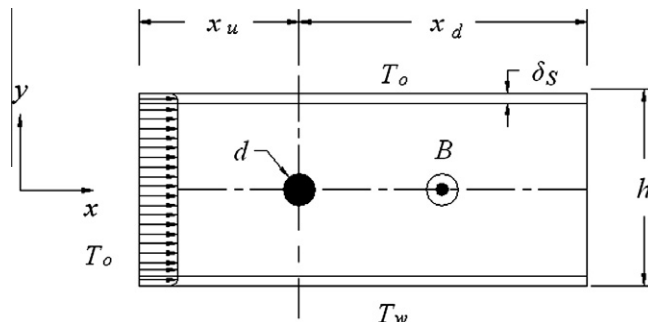


Fig. 1. Schematic representation of the system under investigation. The magnetic field B acts in the out-of-plane direction, parallel to the cylinder axis. The quasi-two-dimensional approximation models an out-of-plane channel height of $2a$. δ_s is the thickness of the Shercliff layer, and h and d are the duct width and cylinder diameter, respectively. The blockage ratio $\beta = d/h$, and the width-to-height aspect ratio $h/2a = 2$.

calculation confirmed their contributions were between 500 times and 10^7 times smaller than those of the included terms for applications motivating this study, such as eutectic alloy flows.

The dimensionless parameters Reynolds number, Hartmann number and Peclet number are respectively defined as

$$Re = \frac{U_0 d}{v}, \quad (4)$$

$$Ha = aB \sqrt{\frac{\sigma}{\rho v}}, \quad (5)$$

$$Pe = Re Pr, \quad (6)$$

where v , σ , B and a are the kinematic viscosity, magnetic permeability of the liquid metal, applied magnetic field, and half the out-of-plane duct height, respectively. In this study, a is taken to be $h/4$, following Frank et al. [30].

The local Nusselt number along the lower heated wall of the channel is defined as

$$Nu_w(x, t) = \frac{d}{(T_f - T_w)} \frac{\partial T}{\partial y} |_{wall}. \quad (7)$$

T_f is the bulk fluid temperature, which is calculated using the velocity and temperature distribution as

$$T_f(x, t) = \frac{\int_0^h u T dy}{\int_0^h u dy}, \quad (8)$$

where h is the width of the duct, and u is the streamwise component of velocity.

A time-averaged Nusselt number for heat transfer through the heated wall of the channel is calculated by first taking the time average of the local Nusselt number (\bar{Nu}_w) at each x -station, and then integrating over the length of the heated bottom wall, L , using

$$Nu = \frac{1}{L} \int_0^L \bar{Nu}_w(x) dx. \quad (9)$$

To characterize the effect on the heat transfer due to the addition of a cylinder to the channel, the overall increment of heat transfer is defined as

$$HI = \frac{Nu - Nu_0}{Nu_0} \times 100, \quad (10)$$

where Nu_0 is the time-averaged Nusselt number of the heated region of the duct without the cylinder.

The total drag coefficient is defined based on the drag force per unit span (F_d) on the cylinder, given as

$$C_d = \frac{F_d}{\frac{1}{2} \rho U_0^2 d} \quad (11)$$

and the wake oscillation frequency f is parameterized by the Strouhal number

$$St = \frac{fd}{U_0}. \quad (12)$$

The flow and heat transfer characteristics are investigated for the quasi two-dimensional channel shown in Fig. 1 for $50 \leq Re \leq 3000$, $0 \leq Ha \leq 1200$, and $0.1 \leq \beta \leq 0.4$. A Prandtl number $Pr = 0.022$ is used throughout, representative of the eutectic alloy GaInSn.

3. Numerical methodology

A nodal spectral-element method is used to discretise the governing flow and energy equations in space, and a third-order scheme based on backwards differentiation is employed for time integration [37]. The spectral element method is similar to the finite element method, in that the fluid domain is divided into a

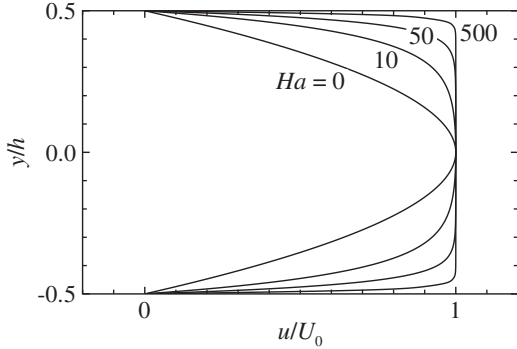


Fig. 2. Normalized base flow velocity profile at Hartmann numbers as indicated.

mesh of individual elements. However, instead of employing a low-order (e.g. linear) basis over each element, a high-order polynomial basis is instead used, permitting very rapid convergence with increasing polynomial degree [37]. The code is an in-house formulation, which has been validated against experimental data [33] and a separate implementation of a similar algorithm [38], and has previously been employed to study channel flows [39].

A constant reference pressure is imposed at the outlet, and a high-order Neumann condition is imposed on the Dirichlet velocity boundaries to preserve the third-order time accuracy of the scheme. An analytical solution exists for quasi-two-dimensional magnetohydrodynamic flow in an unobstructed plane channel. Fig. 2 plots these profiles at a range of Hartmann number, which provides the boundary condition imposed at the channel inlet in this study. At $Ha = 0$ the familiar quadratic profile for Poiseuille flow is found, and as Ha increases, the profile becomes fuller, flattening towards a “top-hat” profile as $Ha \rightarrow \infty$. No-slip boundary conditions for velocity are imposed on the side walls and the cylinder. The temperature of the incoming stream and top wall is taken as T_o , and at the bottom wall as T_w . The cylinder is thermally insulated (a zero normal temperature gradient is imposed at its surface).

A thorough grid resolution study was performed to ensure adequate domain sizes, and spatial and temporal resolutions to accurately resolve all features of the flow field for the Reynolds numbers, the Hartmann numbers and the blockage ratios under consideration in this study. For each blockage ratio, three families of meshes were tested. The drag coefficient (C_d) and the Strouhal frequency of vortex shedding (St) were monitored, as they are known to be sensitive to the domain size and resolution. The upstream and downstream domain length chosen for this study for blockage ratios $\beta = 0.1$ and $\beta = 0.4$ are shown in Table 1. Elements with polynomial degree 7 were used, and parameters $Re = 3000$ and $Ha = 1200$ were chosen to produce periodic flows on the test meshes at each blockage ratio. A difference of less than 1% was found when comparing values of St and C_d between the M_2 and M_3 meshes. Based on this, the M_2 mesh sizing was used hereafter for all blockage ratios.

The spatial resolution study has been performed by varying the element polynomial degree from 4 to 9, while keeping the macro-

element distribution unchanged. Again, the parameters St and C_d were monitored. To ensure uncertainty due to spatial resolution was smaller than that due to domain size, a target of 0.3% uncertainty was desired, and this was found to be achieved with polynomial degree 7, which is used hereafter.

4. Results and discussion

4.1. Validation of the numerical system

Validation was performed against published results to ensure the accuracy of the present formulation and model. The first test concerns the critical Reynolds number (Re_c) and associated Strouhal number (St_c) at the transition from steady to unsteady flow in a zero- Ha flow (i.e. no magnetic field). Results are compared with the published numerical results of Chen et al. [7] and Sahin and Owens [13] in Fig. 3, and an exceptionally close agreement is observed. Critical Reynolds numbers were determined using a linear stability analysis below, and direct numerical simulation above, transition, and extrapolating instability growth rates and mode amplitudes, respectively, to zero.

Computed Nusselt numbers for heat transfer with $Pr = 0.7441$ at blockage ratios of 0.1 and 0.2 are compared against both a theoretical curve [11] and numerical results [15] in Fig. 4. Again, a very good agreement with published data is found.

The third test concerned Re_c under the influence of a magnetic field. Results are compared with experimental results from Frank et al. [30] in Fig. 5(a), which again exhibits a close agreement. The close fit of the present data to that of Frank et al. [30] confirms that the trend is not in fact linear. According to Landau model theory [40], which provides a means for studying the non-linear behavior near the transition Reynolds number, on a plot of $d\log|A|/dt$ against $|A|^2$ (Fig. 5(b)), the value at $|A|^2 = 0$ corresponds to the linear growth rate of instability, and the sign of the gradient at this point determines the non-linear evolution characteristics of

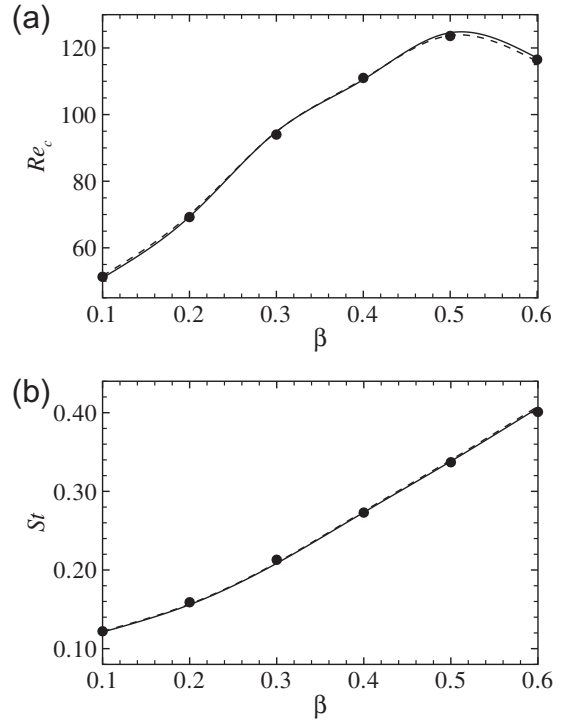


Fig. 3. (a) Re_c and (b) St_c plotted against β . Symbols show the present data, while solid and dashed lines show data published in [13,7], respectively.

Table 1

Domain lengths defining the meshes. N_{el} is the number of elements, and x_u and x_d describe the inlet and outlet domain sizes, respectively.

	$\beta = 0.1$			$\beta = 0.4$		
	M_1	M_2	M_3	M_1	M_2	M_3
N_{el}	1172	1340	1484	1052	1196	1308
x_u	5	8	12	5	8	12
x_d	15	25	40	15	25	40

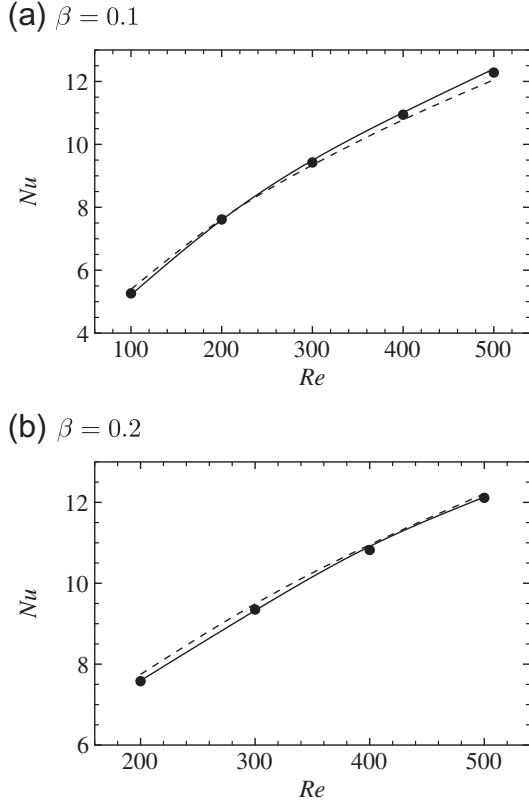


Fig. 4. Comparison of average Nusselt number over the surface of the cylinder with the results from other studies at different Reynolds numbers for the case without a magnetic field for blockage ratios. Symbols show the present results, while solid and dashed lines show data from [15,11], respectively.

the instability. A positive gradient indicates a subcritical bifurcation, which permits hysteresis (bi-stability) in the vicinity of the transition; a negative gradient indicates a supercritical bifurcation, which does not exhibit hysteresis. Fig. 5(b) demonstrates that this transition is supercritical. Frank et al. [30] reported that no evidence of hysteresis was observed, which is confirmed by the Landau modeling of the transition carried out here.

4.2. Fluid flow

Limited data relating Re_c , β and Ha exists in the literature. A comprehensive coverage of the parameter space has therefore been computed, and the results are plotted in Fig. 6. For a given β , Re_c is found to increase with increasing Ha . The increase in Re_c is more pronounced at high Ha and β . This is attributed to the effect of Ha and β which delay the transition from steady to periodic flow regimes, resulting in the enhanced stability of the flow. Higher Hartmann number (i.e. a stronger magnetic field) acts to dampen transverse fluctuations in the channel, which delays transition, resulting in a higher Re being required to invoke transition. In addition, as the cylinder moves closer to the confined walls (higher blockage ratios), the interaction between the wall boundary layer and that of the cylinder suppresses the wake instability from the cylinder.

For a constant Hartmann number, Re_c varies strongly with β at small blockage ratios ($\beta \lesssim 0.3$). Beyond $\beta \gtrsim 0.4$, though, Re_c varies only slightly with β . This may be attributed to the fact that as the lateral walls approach the cylinder, the local acceleration of the flow near the cylinder causes it to experience a high-Re flow, making it more unstable.

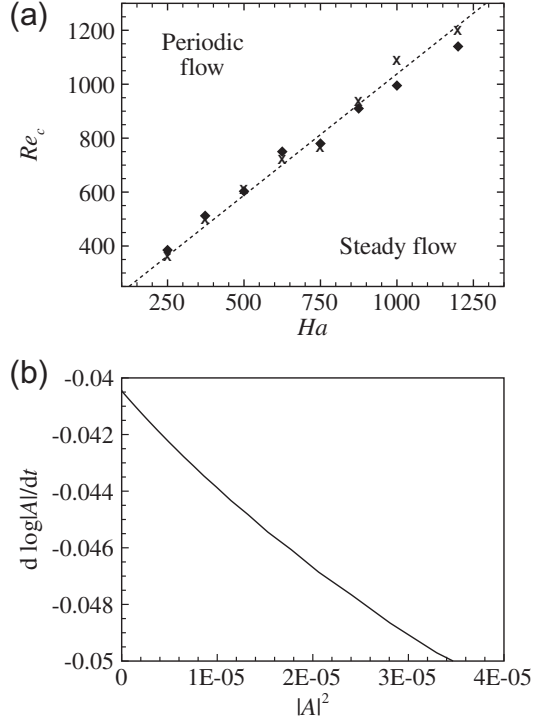


Fig. 5. (a) A plot of Re_c against Ha at $\beta = 0.1$, where \blacklozenge and \times show the present data and experimental data from [30], respectively, and the dotted line is a linear fit proposed by Frank et al. [30]. (b) The time derivative of mode amplitude logarithm plotted against the square of the amplitude for $Ha = 500$ and $\beta = 0.1$, demonstrating supercritical behavior.

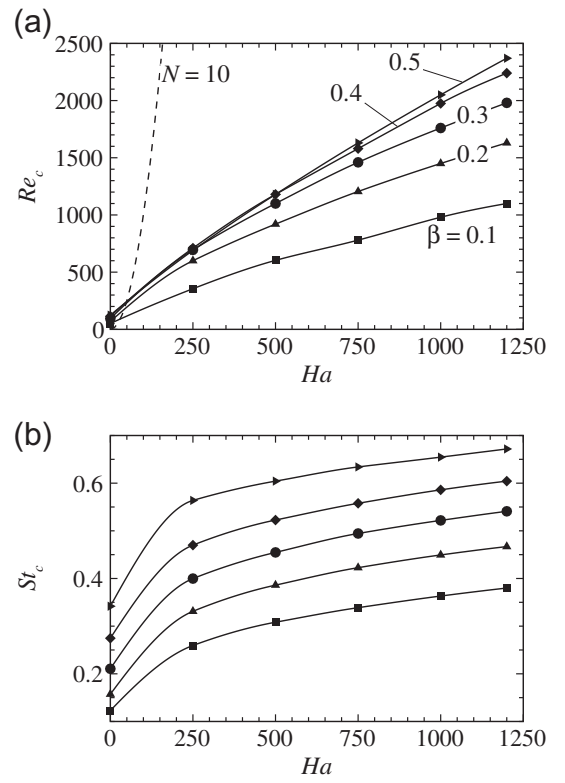


Fig. 6. (a) Re_c and (b) St_c plotted against Ha at blockage ratios as indicated. The dotted line shows the $N = 10$ parabola: the data predominantly lies to the right of that curve, demonstrating the suitability of the quasi-two-dimensional assumption (as $N \gg 1$).

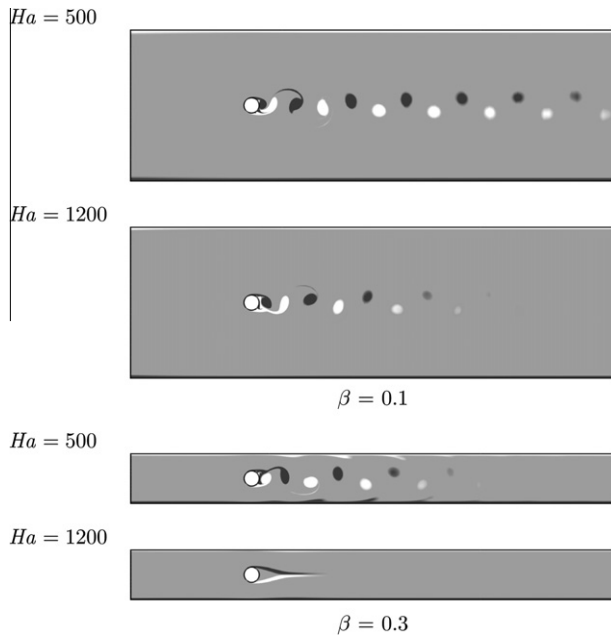


Fig. 7. Vorticity contour plots for $Re = 2000$, β of 0.1 and 0.3 at low and high Hartmann number. Contour levels are displayed between $-2 \leq \omega \leq 2$, with dark and light contours representing negative and positive vorticity, respectively.

Fig. 7 illustrates instantaneous vorticity fields at $Re = 2000$, Hartmann numbers $Ha = 500$ and 1200 , and different blockage ratios. For $\beta = 0.1$, the structure of the Kármán vortex street consists of regular positive and negative vortices shed alternately from the shear layers either side of the cylinder. At high Hartmann number, $Ha = 1200$, the vortices diffuse rapidly as they convect downstream. This was found to be similar to the behaviour at $\beta = 0.2$ (not shown).

For $\beta = 0.3$, and Hartmann number of 500, boundary layer entrainment from the walls (the Shercliff layers) occurs downstream of the cylinder. The vortex street comprises regular vortices shed from the cylinder. The boundary-layer detachment from the walls was observed to increase gradually as the blockage ratio increases through 0.4 and 0.5 at $Ha = 500$ (not shown). Vorticity is drawn into the channel and interacts with the Kármán vortex street, which creates an obstacle that impedes its motion. For $\beta \geq 0.3$ at $Ha = 1200$ vortex shedding is completely suppressed (**Fig. 8**). At $\beta = 0.4$ and 0.5, the recirculation region has almost constant length and separation angle, and the shape of the circulation cone changes little.

The momentum equation of the quasi-two-dimensional Navier–Stokes equations provides insight into the rate of vorticity decay in the wake. Taking the curl of Eq. (2), and recognizing that the velocity field \mathbf{u} is two-dimensional, gives:

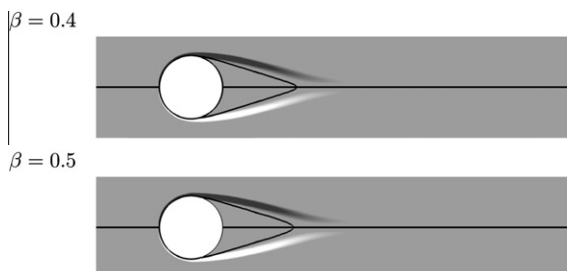


Fig. 8. Plots showing contours of vorticity for $Re = 2000$ and at a Hartmann number of 1200 . Contour levels are displayed between $-2 \leq \omega \leq 2$, with dark and light contours showing negative and positive vorticity, respectively. The recirculation bubble is identified by a contour line through $u = 0$.

$$\frac{D\omega}{Dt} = \frac{1}{Re} \nabla^2 \omega - \frac{d}{a} \frac{Ha}{Re} \omega, \quad (13)$$

where ω is vorticity. The first term is the material derivative, the second term is the viscous diffusion term, and the third term is the Hartmann friction term. As a first approximation, for high Reynolds and Hartmann numbers,

$$\frac{D\omega}{Dt} \approx -\frac{d}{a} \frac{Ha}{Re} \omega, \quad (14)$$

which implies for a convecting packet of vorticity that

$$\frac{d(\log_e \omega)}{dt} \approx -\frac{d}{a} \frac{Ha}{Re}. \quad (15)$$

The peak vorticity magnitude (ω_{peak}) in an individual wake vortex was recorded as it convected downstream in each of the $\beta = 0.1$ flows shown in **Fig. 7**. These vorticity decay time histories are plotted in **Fig. 9**. At $\beta = 0.1$ and $Re = 2000$, the gradients predicted by Eq. (15) for $Ha = 500$ and 1200 are -0.1 and -0.24 , respectively. These are extremely close to the gradients -0.103 and -0.241 found for the least-squares linear fits to the data in **Fig. 9**.

The variation of the time history of the lift coefficient with Hartmann number at different blockage ratios and $Re = 2000$ is shown in **Fig. 10**. At $\beta = 0.1$, the lift coefficient maintains a time-dependent oscillation at $Ha = 500$ and 1200 . However, at $Ha = 1200$ and $\beta = 0.4$, no oscillation is detected as vortex shedding is suppressed.

Fig. 11 presents the effect of the Hartmann number on the time-averaged drag coefficient, C_d , for different blockage ratios. For all β , it is found that C_d first decreases then subsequently increases with an increase in $Re/Ha^{0.8}$. Dousset and Pothérat [32] demonstrated for $\beta = 0.25$ that at low values of $Re/Ha^{0.8}$, data collapses onto a universal curve. Similar collapses are observed at each blockage ratio, though to distinct curves—hence the collapse is blockage-ratio dependent. At higher $Re/Ha^{0.8}$, the drag coefficient increases, and displays a dependence on Hartmann number. All data presented in **Fig. 11** represents time-dependent flows. In the low- $Re/Ha^{0.8}$ regime, the flow dynamics is dominated by Hartmann damping. Conversely, at higher $Re/Ha^{0.8}$, Hartmann damping is no longer dominant, and the wake resembles vortex shedding in the absence of a magnetic field. Examples of these regimes are, respectively, the $Ha = 1200$ and $Ha = 500$ flows at $\beta = 0.1$ plotted in **Fig. 7**.

4.3. Heat transfer

Fig. 12 presents the distribution of instantaneous temperature contours for blockage ratios $\beta = 0.2$, 0.3 and 0.4, and Hartmann numbers $Ha = 500$ and 1200 at $Re = 2000$. For all β , when $Ha = 500$ the temperature fields are time-dependent because the

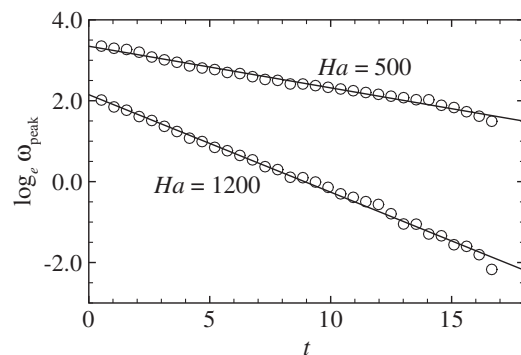


Fig. 9. Time history of the natural logarithm of peak vorticity in a vortex convecting down the wake. Symbols show data points calculated at $\beta = 0.1$, $Re = 2000$, and Hartmann numbers $Ha = 500$ and 1200 . Lines of best fit have gradients of -0.103 and -0.241 .

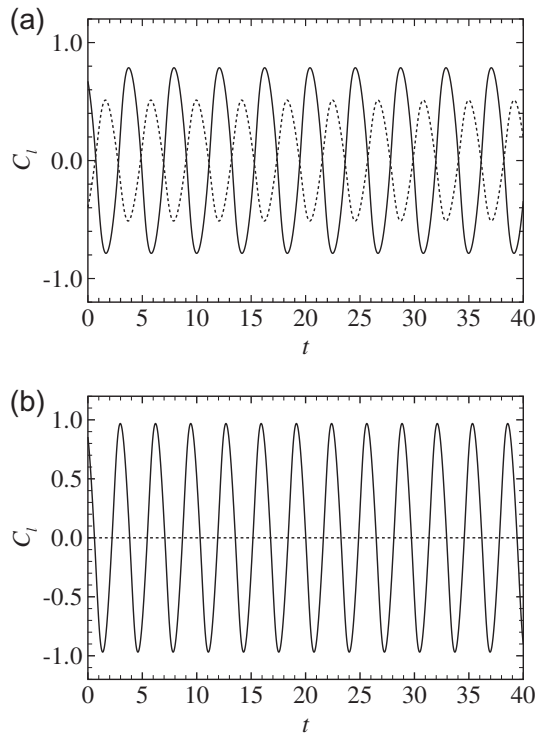


Fig. 10. Time history of lift force coefficient for a blockage ratio of 0.1 (a) and 0.4 (b) at Hartmann numbers $Ha = 500$ (solid line) and 1200 (dashed line) for $Re = 2000$.

flow is unsteady. As the blockage ratio is further increased, the velocity of the flow near the heated wall increases. Therefore, the low-temperature fluid is transported toward the hot region of the channel and the high-temperature fluid near the heated wall is convected away to mix with the low-temperature fluid. Consequently, the heat transfer is enhanced remarkably. However, as Ha is increased to 1200, the unsteadiness in the flow is suppressed at $\beta = 0.2$, and the flow is steady as β increases to 0.3. This increases the thickness of the thermal boundary layer, and hence the temperature gradient along the heated wall decreases.

Fig. 13 shows the effect of the blockage ratio on the time-averaged Nusselt number of the heated wall (Nu) for Hartmann numbers $Ha = 500$ and 1200 at $Re = 2000$ and 3000. The heat transfer is shown to be higher at higher Reynolds numbers. At $Ha = 500$, there is a remarkable increase in Nu for both Reynolds numbers as β is increased from 0.1 to 0.4. The increase is more pronounced at $\beta \geq 0.2$. However, Nu reduces as Hartmann number is increased to $Ha = 1200$.

To gauge the improvement to the heat transfer generated by placing a cylinder in the duct, the percentage increment of the overall heat transfer is calculated using Eq. (10) for the flows considered in this study. For $Re = 2000$ and $Ha = 500$, the percentage increment for $0.1 \leq \beta \leq 0.4$ ranges between 3% and 89%. At $Ha = 1200$, the increments are smaller, ranging up to 25%. For $Re = 3000$, the overall heat transfer increments range between 7% and 128% at $Ha = 500$, and between 6% and 34% at $Ha = 1200$. Thus at $Ha \approx 500$ and $Re \gtrsim 3000$, in channels with blockage ratios $\beta \approx 0.4$, heat transfer is enhanced by more than 100% by placing a cylinder within the channel.

Fig. 14 shows the distribution of the local Nusselt number along the heated wall (Nu_w) as a function of stream-wise coordinate x for different Hartmann numbers at $Re = 2000$. The effect of Hartmann number is found to be negligible for small blockage ratio ($\beta = 0.1$). Similarly, at $\beta = 0.2$, the variation of the local Nusselt number with Hartmann number is independent, except that of $Ha = 500$.

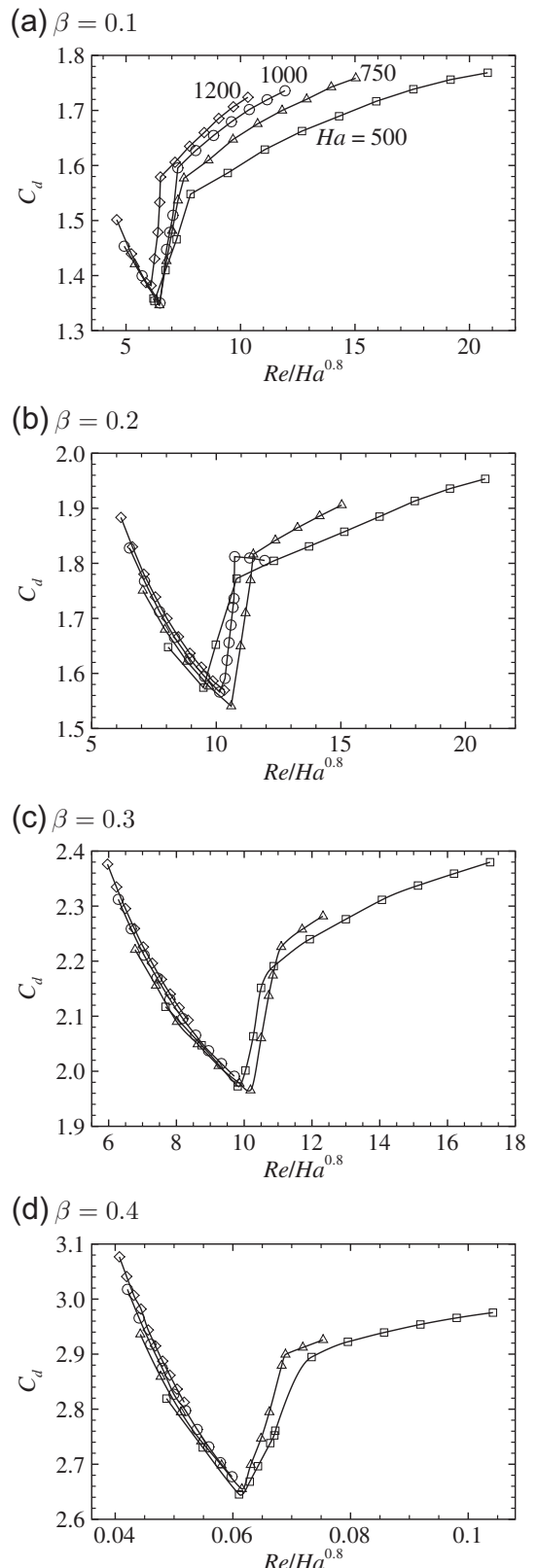


Fig. 11. Time-averaged drag coefficients as a function of $Re/Ha^{0.8}$ at different Hartmann numbers and blockage ratios as indicated.

However, as the blockage ratio increases further from 0.2 to 0.4, the change in the distribution of Nu_w is remarkable with changing Hartmann number. The change is more pronounced at low Hartmann number. The plot also demonstrates that the curves collapse

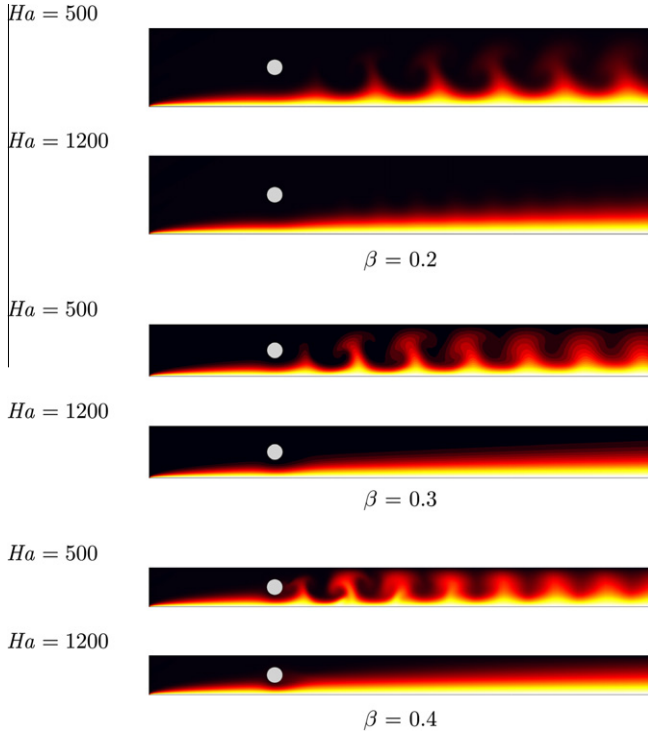


Fig. 12. Instantaneous dimensionless temperature contours at $Re = 2000$ for $\beta = 0.2$, $\beta = 0.3$ and $\beta = 0.4$ at low and high Hartmann number. Light and dark shading shows hot and cold fluid, respectively.

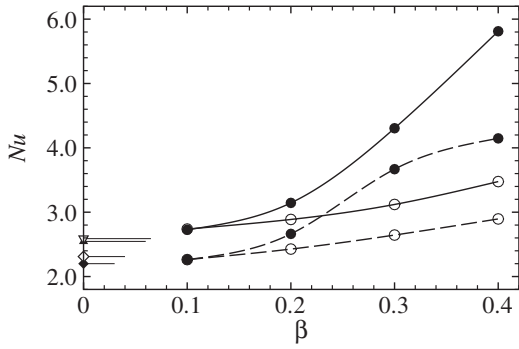


Fig. 13. Effect of Hartmann number and blockage ratio on the time-averaged Nusselt number for Reynolds numbers $Re = 2000$ (dashed lines) and 3000 (solid lines). Solid symbols show $Ha = 500$ and open symbols show $Ha = 1200$. For reference, Nusselt number values for the channel without a cylinder present are also provided: (\blacklozenge , \diamond) represent $Re = 2000$ at $Ha = 500$ and 1200 , respectively. (\blacktriangle , \triangledown) represent $Re = 3000$ at $Ha = 500$ and 1200 , respectively.

to a single curve at high Hartmann number and small blockage ratio.

In magnetohydrodynamic channel flows, the pressure drop becomes large at high Hartmann number. Thus in the context of this study it is prudent to consider the additional pressure drop penalty incurred by adding a cylinder to the channel. In Fig. 15, the pressure drop penalty is plotted. The data demonstrates that at low blockage, there is only a small increase in pressure drop due to the addition of the cylinder. However, as the blockage increases (particularly through $\beta = 0.3$ and 0.4), the increase in pressure drop is also more substantial. The pressure drop penalty displays an increased dependence on Hartmann number as the blockage ratio increases, with increasing Hartmann number resulting in an increased pressure drop penalty. Demonstrating the significant effect of Hartmann number on the pressure drop penalty, at $Ha = 500$

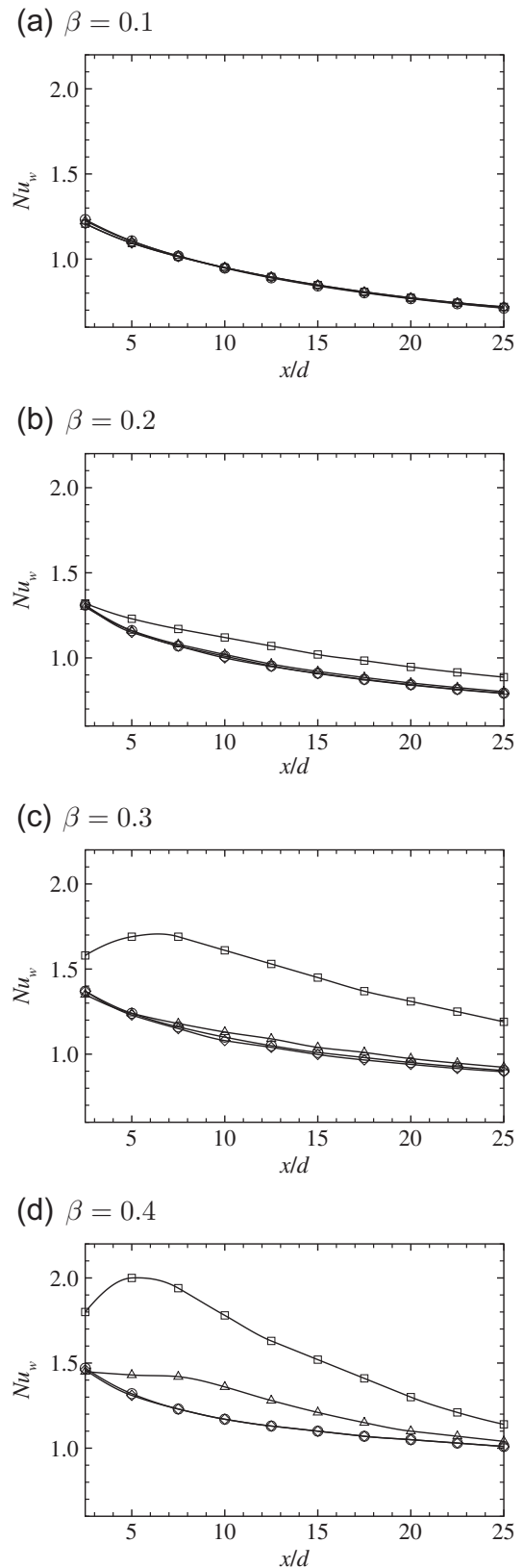


Fig. 14. Local Nusselt number over the heated surface of the side wall as a function of x at $Re = 2000$ and different Hartmann numbers (symbols as per Fig. 11), and blockage ratios as indicated.

the penalty at $\beta = 0.4$ is 11 times that at $\beta = 0.1$, and at $Ha = 1200$ this ratio increases to 16. The blockage effect rapidly comes into effect between $\beta = 0.2$ and 0.3 . Between these blockage ratios, the

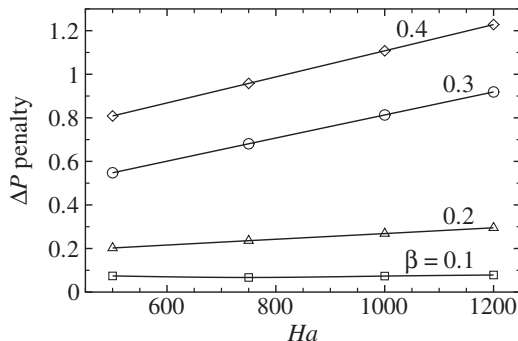


Fig. 15. Pressure drop penalty at $Re = 2000$ due to inclusion of a circular cylinder within the duct, plotted against Ha . The pressure drop penalty is the difference in pressure drop across identical channels with and without a circular cylinder. Blockage ratios $\beta = 0.1$ (□), 0.2 (△), 0.3 (○) and 0.4 (◇) are shown. Splines are included for guidance.

gradient of pressure drop penalty with Hartmann number increases by a factor of 4, whereas a much more modest increase is observed as blockage ratio increases to 0.4.

5. Conclusion

The present study numerically investigates the characteristics of liquid metal flow and heat transfer past a circular cylinder in a rectangular duct under a strong magnetic field parallel to the cylinder using a spectral-element method. Under these conditions, the flow is quasi-two-dimensional and the modified Navier–Stokes equations are solved in a two-dimensional domain. The numerical simulations have been performed over the range of Reynolds numbers $100 \leq Re \leq 3000$, Hartmann numbers $500 \leq Ha \leq 1200$, and blockage ratios $0.1 \leq \beta \leq 0.5$. The transition Reynolds number from steady to unsteady flow past a circular cylinder confined in a plane channel is determined as a function of Ha and β . Parameters are chosen to represent a channel with aspect ratio (width-to-height) of 2, and the effect of Hartmann layers on the out-of-plane channel walls are described through the Hartmann friction term added to the Navier–Stokes equations.

The critical Reynolds number at which the transitions from steady to unsteady flow occurs was found to increase with increasing Ha for all values of β . At $Re = 2000$, $\beta \leq 0.2$ and $Ha = 500$ and 1200, the structure of the Kármán vortex street consists of regular positive and negative vortices shed respectively from the bottom and the top of the cylinder. As β is increased to 0.3, at $Ha = 500$, the boundary layer detachment from the side wall of the duct occurs downstream of the cylinder. The detachment of the boundary layer increased gradually as β increases further to 0.4 and 0.5. For $\beta \geq 0.3$, at $Ha = 1200$, vortex shedding is completely suppressed.

For all β , it is found that the drag coefficient C_d first decreases and then increases as Reynolds number is increased. The viscous contribution to the drag coefficient for the cylinder was much smaller than the pressure drag coefficient. Therefore, C_d is dominated by the part of the pressure forces. This is attributed to the effect of Hartmann friction and the confinement of the walls that delay the transitions of the flow to a higher Reynolds number. As a result, the viscous contribution is much smaller than that of the pressure. Also, for all β , it was found that at each blockage ratio the curves collapse to universal curves at lower values of $Re/Ha^{0.8}$.

The heat transfer rate is strongly dependent on the Hartmann number and blockage ratio. For small Hartmann number, it increases significantly as blockage ratio is increased. However, there is a gradual increase in the Nusselt number for high Hartmann

number as blockage ratio is increased. Overall, though, the enhancement of heat transfer was significantly augmented with increasing blockage ratio, in some cases by more than twofold.

The effect of the Hartmann number on the local Nusselt number from the heating wall of the duct, Nu_w , is found to be negligible for small blockage ratios. However, for high blockages, the change in Nu_w was found to be significant with different Hartmann number.

The pressure drop penalty incurred by adding a cylinder to the channel is found to increase with both blockage ratio and Hartmann number, and the penalty is increasingly dependent on Hartmann number at higher blockage ratios.

References

- [1] S. Münevver, Magnetohydrodynamic flow in a rectangular duct, *Int. J. Numer. Meth. Fluids* 7 (1987) 697–718.
- [2] I.R. Kirillov, C.B. Reed, L. Barleon, K. Miyazaki, Present understanding of MHD and heat transfer phenomena for liquid metal blankets, *Fusion Eng. Des.* 27 (1995) 553–569.
- [3] O. Lielausis, Liquid-metal magnetohydrodynamics, *Atomic Energy Rev.* 13 (1975) 527–581.
- [4] C.H.K. Williamson, Vortex dynamics in the cylinder wake, *Annu. Rev. Fluid Mech.* 28 (1996) 477–539.
- [5] M.M. Zdravkovich, *Flow Around Circular Cylinders: A Comprehensive Guide Through Flow Phenomena, Experiments, Applications, Mathematical Models, and Computer Simulations*, Oxford University Press, 2003.
- [6] M. Coutanceau, R. Bouard, Experimental determination of the main features of the viscous flow in the wake of a circular cylinder in uniform translation. Part 1. steady flow, *J. Fluid Mech.* 79 (1977) 231–256.
- [7] J.H. Chen, W.G. Pritchard, S.J. Tavener, Bifurcation for flow past a cylinder between parallel planes, *J. Fluid Mech.* 284 (1995) 23–41.
- [8] M. Behr, D. Hasteirter, S. Mittal, T.E. Tezduyar, Incompressible flow past a circular cylinder: dependence of the computed flow field on the location of the lateral boundaries, *Comput. Meth. Appl. Mech. Eng.* 123 (1995) 309–316.
- [9] P. Agostopoulos, G. Iliadis, S. Richardson, Numerical study of the blockage effects on viscous flow past a circular cylinder, *Int. J. Numer. Meth. Fluids* 22 (1996) 1061–1074.
- [10] L. Zovatto, G. Pedrizzetti, Flow about a circular cylinder between parallel walls, *J. Fluid Mech.* 440 (2001) 1–25.
- [11] W.A. Khan, J.R. Yovanovich, M.M. Culham, Fluid flow and heat transfer from a cylinder between parallel planes, *J. Thermophys. Heat Transfer* 18 (2004) 395–403.
- [12] J. Chakraborty, N. Verma, R.P. Chhabra, Wall effects in flow past a circular cylinder in a plane channel: a numerical study, *Chem. Eng. Proc.* 43 (2004) 1529–1537.
- [13] M. Sahin, R.G. Owens, A numerical investigation of wall effects up to high blockage ratios on two-dimensional flow past a confined circular cylinder, *Phys. Fluids* 16 (2004) 1305–1320.
- [14] K.A. Cliffe, S.J. Tavener, The effect of cylinder rotation and blockage ratio on the onset of periodic flows, *J. Fluid Mech.* 501 (2004) 125–133.
- [15] S. Mettu, N. Verma, R. Chhabra, Momentum and heat transfer from an asymmetrically confined circular cylinder in a plane channel, *Heat Mass Transfer* 42 (2006) 1037–1048.
- [16] J.A. Shercliff, Some duct flow problems at high Hartmann number, *Zeit. Angew. Math. Phys. (ZAMP)* 26 (1975) 537–548.
- [17] P.A. Davidson, The role of angular momentum in the magnetic damping of turbulence, *J. Fluid Mech.* 336 (1997) 123–150.
- [18] A. Pothierat, J. Sommeria, R. Moreau, An effective two-dimensional model for MHD flows with transverse magnetic field, *J. Fluid Mech.* 424 (2000) 75–100.
- [19] J. Sommeria, R. Moreau, Why, how, and when, MHD turbulence becomes two-dimensional, *J. Fluid Mech.* 118 (1982) 507–518.
- [20] T. Alboussiere, V. Uspenski, R. Moreau, Quasi-2d MHD turbulent shear layers, *Exp. Therm. Fluid Sci.* 20 (1999) 19–24.
- [21] O.V. Andreev, Y. Kolesnikov, MHD instabilities at transverse flow around a circular cylinder in an axial magnetic field, in: *Third International Conference on Transfer Phenomena in Magnetohydrodynamic and Electroconducting Flows*, Aussois, France, pp. 205–210.
- [22] U. Burr, L. Barleon, U. Müller, A. Tsinober, Turbulent transport of momentum and heat in magnetohydrodynamic rectangular duct flow with strong sidewall jets, *J. Fluid Mech.* 406 (2000) 247–279.
- [23] R. Klein, A. Pothierat, A. Alferenok, Experiment on a confined electrically driven vortex pair, *Phys. Rev. E* 79 (2009) 016304.
- [24] L. Buhler, Instabilities in quasi-two-dimensional magnetohydrodynamic flows, *J. Fluid Mech.* 326 (1996) 125–150.
- [25] Y.B. Kolesnikov, A.B. Tsinober, Experimental investigation of two-dimensional turbulence behind a grid, *Fluid Dyn.* 9 (1974) 621–624.
- [26] J. Moreau, R. Sommeria, Electrical driven vortices in a strong magnetic field, *J. Fluid Mech.* 189 (1988) 553–569.
- [27] L. Kit, S. Turntaev, A.B. Tsinober, Investigation with a conducting anemometer of the effect of magnetic field on disturbances of cylinder, *Magnetohydrodynamics* 6 (1970) 35–40.

- [28] Y.B. Kolesnikov, A.B. Tsinober, Two-dimensional turbulent flow behind a circular cylinder, *Magneto hydrodynamics* 3 (1972) 300–307.
- [29] D.D. Papailiou, Magneto-fluid-mechanic turbulent vortex streets, in: Fourth Beer-Sheva Seminar on MHD Flows and Turbulence, AIAA, 1984, pp. 152–173.
- [30] M. Frank, L. Barleon, U. Muller, Visual analysis of two-dimensional magnetohydrodynamics, *Phys. Fluids* 13 (2001) 2287–2295.
- [31] B. Muck, C. Gunther, U. Muller, L. Buhler, Three-dimensional MHD flows in rectangular ducts with internal obstacles, *J. Fluid Mech.* 418 (2000) 265–295.
- [32] V. Dousset, A. Pothérat, Numerical simulations of a cylinder wake under a strong axial magnetic field, *Phys. Fluids* 20 (2008) 017104.
- [33] G.J. Sheard, T. Leweke, M.C. Thompson, K. Hourigan, Flow around an impulsively arrested circular cylinder, *Phys. Fluids* 19 (2007) 083601.
- [34] G.J. Sheard, M.P. King, The influence of height ratio on Rayleigh-number scaling and stability of horizontal convection, *Appl. Math. Model.* (2011), doi:[10.1016/j.apm.2010.09.041](https://doi.org/10.1016/j.apm.2010.09.041).
- [35] M.A. Hossain, Viscous and Joule heating effects on MHD-free convection flow with variable plate temperature, *Int. J. Heat Mass Transfer* 35 (1992) 3485–3487.
- [36] H.S. Yoon, H.H. Chun, M.Y. Ha, H.G. Lee, A numerical study on the fluid flow and heat transfer around a circular cylinder in an aligned magnetic field, *Int. J. Heat Mass Transfer* 47 (2004) 4075–4087, doi:[10.1016/j.ijheatmasstransfer.2004.05.015](https://doi.org/10.1016/j.ijheatmasstransfer.2004.05.015). Note 0017-9310.
- [37] G.E. Karniadakis, M. Israeli, S.A. Orszag, High-order splitting methods for the incompressible Navier–Stokes Eqs, *J. Comput. Phys.* 97 (1991) 414–443.
- [38] H.M. Blackburn, G.J. Sheard, On quasi-periodic and subharmonic Floquet wake instabilities, *Phys. Fluids* 22 (2010) 031701.
- [39] A. Neild, T.W. Ng, G.J. Sheard, M. Powers, S. Oberti, Swirl mixing at microfluidic junctions due to low frequency side channel fluidic perturbations, *Sens. Act. B: Chem.* 150 (2010) 811–818.
- [40] M. Provansal, C. Mathis, L. Boyer, Bénard–von Kármán instability: transient and forced regimes, *J. Fluid Mech.* 182 (1987) 1–22.